Draft version October 23, 2012
Preprint typeset using LaTeX style emulateapj v. 12/16/11

SLAC-PUB-15314

RHAPSODY: II. SUBHALO PROPERTIES AND THE IMPACT OF TIDAL STRIPPING FROM A STATISTICAL SAMPLE OF CLUSTER-SIZE HALOS

Hao-Yi Wu,[1,2] Oliver Hahn,[1,3] Risa H. Wechsler,[1] Peter S. Behroozi,[1] Yao-Yuan Mao[1]
[1]Kavli Institute for Particle Astrophysics and Cosmology; Physics Department, Stanford University, Stanford, CA, 94305
SLAC National Accelerator Laboratory, Menlo Park, CA, 94025
[2]Physics Department, University of Michigan, Ann Arbor, MI 48109; hywu@umich.edu
[3]Institute for Astronomy, ETH Zurich, CH-8093 Zürich, Switzerland

Draft version October 23, 2012

ABSTRACT

We discuss the properties of subhalos in cluster-size halos, using a high-resolution statistical sample: the Rhapsody simulations introduced in Wu et al. (2012). We demonstrate that the criteria applied to select subhalos have significant impact on the inferred properties of the sample, including the scatter in the number of subhalos, the correlation between the subhalo number and formation time, and the shape of subhalos' spatial distribution and velocity structure. We find that the number of subhalos, when selected using the peak maximum circular velocity in their histories (a property expected to be closely related to the galaxy luminosity), is uncorrelated with the formation time of the main halo. This is in contrast to the previously reported correlation from studies where subhalos are selected by the current maximum circular velocity; we show that this difference is a result of the tidal stripping of the subhalos. We also find that the dominance of the main halo and the subhalo mass fraction are strongly correlated with halo concentration and formation history. These correlations are important to take into account when interpreting results from cluster samples selected with different criteria. Our sample also includes a fossil cluster, which is presented separately and placed in the context of the rest of the sample.

Keywords: cosmology: theory — dark matter — galaxies: clusters: general — galaxies: halos — methods: N-body simulations

1. INTRODUCTION

The abundance and spatial distribution of galaxy clusters in the universe have played an essential role in determining cosmological parameters. These properties are sensitive to cosmic expansion and the large-scale structure growth rate, making clusters complementary to other cosmological probes (see, e.g., Allen et al. 2011 and Weinberg et al. 2012 for recent reviews, and references therein). Among multi-wavelength cluster surveys, optical surveys provide the largest statistical power in terms of the number of identified clusters; this number will dramatically increase with the next generation of wide area surveys, including PanSTARRS[1], DES[2], Euclid[3], and LSST[4]. However, the precision cosmology that can potentially be achieved will be limited by the systematic effects involved, including cluster identification and centering (e.g., Rykoff et al. 2012), the normalization and scatter of the richness–mass relation (e.g., Rozo et al. 2009, 2011), orientation and projection effects (e.g., Cohn et al. 2007; White et al. 2010; Erickson et al. 2011), cross-comparison with multi-wavelength data (Rozo et al. 2012), as well as uncertainties in theoretical calibrations of halo statistics (Wu et al. 2010).

To quantify the systematic effects inherent in the measurements of galaxy clusters, it is essential to generate a simulated sample of clusters that is comparable to the relevant observations. A common procedure is to use dark matter-only N-body simulations to predict the distribution of dark matter particles and halos, and then relate halos and subhalos to the observed galaxy clusters and their member galaxies (e.g., Kravtsov et al. 2004; Zheng et al. 2005). However, resolving subhalos in cluster-size halos comparable to the observable limits and associating them with galaxies presents additional challenges. As described by the hierarchical structure formation paradigm, subhalos accrete onto the main halo through numerous merger events and have been substantially influenced by the deep gravitational potential of the main halo (e.g., Ghigna et al. 1998; Moore et al. 1998, 1999). Therefore, simulating these subhalos requires high mass and force resolution (e.g., Klypin et al. 1999), improved halo finding (e.g., Onions et al. 2012), as well as a careful modeling of the associated satellite galaxies (e.g., Reddick et al. 2012).

To characterize the galaxy populations in galaxy clusters obtained from deep wide surveys, it is necessary to simulate clusters with high resolution (to resolve the galaxy content to observable limits) and in a large cosmological volume (to obtain a statistical sample), which is computationally challenging. As discussed in Paper I (Wu et al. 2012), in order to achieve large sample size and high resolution simultaneously, we have repeatedly applied a "zoom-in" or multi-resolution simulation technique to develop the Rhapsody sample, which currently includes 96 halos of mass $10^{14.8\pm0.05}h^{-1}\mathrm{M}_\odot$, selected from a cosmological volume of side length 1 h^{-1}Gpc and resimulated with mass resolution $1.3\times10^8h^{-1}\mathrm{M}_\odot$. This sample is currently unique in terms of its sample size and

[1] The Panoramic Survey Telescope & Rapid Response System; http://pan-starrs.ifa.hawaii.edu/
[2] The Dark Energy Survey; http://www.darkenergysurvey.org/
[3] http://sci.esa.int/euclid/
[4] The Large Synoptic Survey Telescope; http://www.lsst.org/

Work supported by US Department of Energy contract DE-AC02-76SF00515.

resolution and occupies a new statistical regime of cluster simulations (see Figure 1 in Paper I). In this second paper, we focus on the subhalo population of the RHAPSODY clusters and give particular attention to the impact of formation history and tidal stripping on subhalos.

The impact of formation history on the observable properties of clusters (e.g., galaxy number and distribution) is important because it can provide extra information or, if not correctly taken into account, introduce bias in cluster mass calibration and in cosmological constraints that depend on the properties of galaxies in clusters. For example, Wu et al. (2008) have shown that if the richness of a cluster (the number of galaxies in a cluster under a certain selection criterion, used as a cluster-mass indicator) is correlated with its formation time, then richness-selected clusters will be impacted by assembly bias (i.e., early forming halos have a higher halo bias), which will in turn impact cluster mass self-calibration and cause systematic errors in the inferred cosmological parameters. Cosmological studies which use information about the halo occupation of galaxies (the number of galaxies inside a halo for a given halo mass) also depend on an understanding of whether this occupation depends on properties other than halo mass. Therefore, it is imperative to characterize these correlations with higher precision using a statistical sample relevant for current and future surveys.

In this paper, we discuss how formation history impacts the subhalo abundance, subhalo mass fraction, and the dominance of the main halo over its subhalos. In particular, we focus on the influence of the specific criteria used to select subhalos from simulations on the inferred properties of the subhalo population thus obtained. One of our main findings is that the correlation between subhalo number and formation time sensitively depends on this selection criterion. If we use a subhalo selection criterion that is insensitive to the stripping of dark matter particles, the subhalo number and halo formation time are not correlated. This result implies that both the halo occupation and the cluster richness for halos of a given mass are not likely to correlate with formation time.

This paper is organized as follows. In §2, we briefly summarize our simulations and halo catalogs, as well as the various subhalo selection criteria that we consider. In §3, we present the statistics of subhalos and the shape of their spatial distribution and velocity ellipsoid. In §4, we discuss how formation time impacts observational signatures of subhalos, including the subhalo mass fraction and the dominance of the main halo. In §5, we focus on the impact of halo formation time and tidal stripping on the number of subhalos. We conclude in §6.

2. HALO CATALOGS

The RHAPSODY sample includes 96 cluster-size halos of mass $M_{\rm vir} = 10^{14.8\pm0.05} h^{-1}{\rm M}_\odot$, re-simulated from a cosmological volume of 1 $h^{-3}{\rm Gpc}^3$. Each halo has been simulated at two resolutions: $1.3\times10^8 h^{-1}{\rm M}_\odot$ (equivalent to 8192^3 particles in this volume), which we refer to as "RHAPSODY 8K" or simply "RHAPSODY"; and $1.0\times10^9 h^{-1}{\rm M}_\odot$ (equivalent to 4096^3 particles in this volume), which we refer to as "RHAPSODY 4K." The simulation parameters are summarized in Table 1 of Paper I.

All simulations in this work are based on a ΛCDM cosmology with density parameters $\Omega_m = 0.25$, $\Omega_\Lambda = 0.75$, $\Omega_b = 0.04$, spectral index $n_s = 1$, normalization $\sigma_8 = 0.8$, and Hubble parameter $h = 0.7$.

2.1. *The Simulations*

The implementation of RHAPSODY can be summarized as follows:

1. Selecting the re-simulation targets: We start from one of the 1 h^{-1}Gpc volumes (named "CARMEN") from the LASDAMAS suite of simulations[5] and select halos in a narrow mass bin $10^{14.8\pm0.05}$ $h^{-1}{\rm M}_\odot$.
2. Generating initial conditions: We use the multi-scale initial condition generator MUSIC (Hahn & Abel 2011) to generate "zoom" initial conditions for each cluster with the second-order Lagrangian perturbation theory.
3. Performing gravitational evolution: We compute the non-linear evolution of each cluster down to $z = 0$ using the public version of GADGET-2 (Springel 2005).
4. Identifying halos and subhalos: We use the adaptive phase-space halo finder ROCKSTAR (Behroozi et al. 2011a) to assemble catalogs of halos and subhalos at 200 output times. ROCKSTAR achieves a particularly high completeness of the subhalo sample.
5. Constructing merger trees: We use the gravitationally consistent merger tree code by Behroozi et al. (2011b) to construct merger trees from the halo/subhalo catalogs.

We kindly refer the reader to § 2 of Paper I for more details on the simulations, the halo and subhalo identification and merger tree generation, as well as the mean values and variances of the various key properties of the main cluster halos in RHAPSODY (given in Table 2 of Paper I).

2.2. *Subhalo selection methods*

Subhalos in cluster-size halos are expected host the observed satellite galaxies in clusters. For each main halo in RHAPSODY, we consider the subhalos within its virial radius, $R_{\rm vir}$ (based on the spherical overdensity calculated with Bryan & Norman 1998 $\Delta_{\rm vir} = \Delta_{94c}$ at z=0). We characterize each subhalo by the maximum circular velocity of the dark matter particles associated with it, $\rm v_{max}$, defined at the radius $r = r_{\rm max}$ that maximizes $\sqrt{GM(<r)/r}$:

$$\rm v_{max} = \sqrt{\frac{GM(<r_{max})}{r_{max}}}\ . \qquad (1)$$

This quantity is often used as a proxy for subhalo mass, since the mass of a subhalo itself is typically not a well defined quantity in the simulations due to ambiguities about how to separate subhalos from the background density of the main halo. We focus on $\rm v_{max}$ at two different epochs during the evolution history of a subhalo:

- $\rm v_0$: the value of $\rm v_{max}$ measured at $z = 0$, a quantity related to the current subhalo mass.

[5] http://lss.phy.vanderbilt.edu/lasdamas/

- v_{pk}: the highest v_{max} value in a subhalo's history, a quantity related to the highest subhalo mass in its entire history.

Since subhalos experience strong tidal stripping after their accretion onto the main halo, the two are not identical. The parameter v_{pk} is more closely related to the luminosity and stellar mass of satellite galaxies than v_0, because the stellar component of a galaxy is denser and less easily stripped than the more extended dark matter component. Even though a halo could lose dark matter particles at its outskirts, the galaxy in its core can remain intact for a longer time. In fact, the satellite galaxy may even continue to grow (e.g., Wetzel et al. 2012). Therefore, a quantity that is unaffected by stripping is expected to provide a better proxy for the stellar mass of galaxies.

In particular, subhalo abundance matching models based on properties that are less impacted by stripping have been shown to better agree with observations. For example, Nagai & Kravtsov (2005) and Conroy et al. (2006) have shown that using v_{ac} (i.e., v_{max} at the time of accretion of the subhalo) when selecting subhalos better reproduces the statistics of observed galaxies. Reddick et al. (2012) have further demonstrated that an abundance matching model based on v_{pk} provides a better fit than either v_0 or v_{ac} to the galaxy two-point correlation function and the conditional stellar mass function for galaxies in groups from the Sloan Digital Sky Survey (SDSS).

In addition to v_{max}, we also investigate the mass of subhalos at two different epochs:

- M_0: the current subhalo mass, defined by the particles bound to the subhalo according to the implementation of ROCKSTAR.
- M_{pk}: the highest mass in a subhalo's entire assembly history.

In general, the difference between M_0 and M_{pk} is analogous to the difference between v_0 and v_{pk}, except that the circular velocity is less affected by stripping than mass is.

It is important to note here that finite resolution in N-body simulations leads to the "overmerging" effect (e.g., Klypin et al. 1999): small subhalos tend to fall below the resolution limit before they merge with the central object. However, the stellar component associated with subhalos is expected to survive longer than the simulated subhalos. A detailed discussion of the resolution dependence of this effect and the associated completeness limits of the subhalo populations will be presented in a separate paper (Wu et al., in preparation).

3. SUBHALO STATISTICS AND DISTRIBUTIONS AT $Z = 0$

In this section, we focus on the statistical properties of the subhalos in RHAPSODY, as well as the shape of the subhalos' spatial distribution and velocity ellipsoid. In particular, we explore the impact of resolution and of the various selection criteria described in the previous section.

3.1. *Subhalo mass function*

The mass function of subhalos has been shown to follow a power law for low mass subhalos and an exponential cutoff for massive subhalos (e.g., Gao et al. 2004; Angulo et al. 2009; Giocoli et al. 2010). In this section, we investigate the validity of this form when using the various criteria for subhalo selection .

Figure 1 shows the number of subhalos above a given threshold of v_0 (left), v_{pk} (middle), and M_0 (right). The blue/red curves correspond to subhalos within R_{vir} of RHAPSODY 8K/4K halos, while the transparent grey curves correspond to individual halos in RHAPSODY 8K. The black curves correspond to all halos and subhalos within 7 h^{-1}Mpc around the center of the main halo, a region where re-simulated halos are well resolved[6]. The blue dashed lines indicate the best-fit power-law slopes of the distribution functions of the 8K sample. We find that the slope of our M_0 function is slightly shallower than De Lucia et al. (2004), Boylan-Kolchin et al. (2010), and Gao et al. (2012), which is plausibly attributed to the different mass definition. At the same time, our v_0 function is in good agreement with the results of Boylan-Kolchin et al. (2010) and Wang et al. (2012) based on Milky Way-size halos. The large halo-to-halo scatter shown here has implications for comparisons of satellite statistics in the Milky Way with simulations, given that thus far these comparisons have been done with a small number of simulated halos. Scatter in the properties of satellites between halos likely reduces the current tension with observations of massive dwarf galaxies (e.g., Purcell & Zentner 2012). A statistical sample for galactic subhalos from simulations, as well as a larger sample of observed systems, is required to verify these results.

The 4K and 8K subhalo mass functions deviate from a power law at different values of v_0 and v_{pk}, clearly indicating the dependence of the completeness limit for all mass proxies on resolution. The gray curves demonstrate the significant scatter in subhalo abundance from halo to halo in our sample. Given this large scatter, we next explore how well the number of subhalos in different bins are correlated, i.e., how sensitive a richness estimator would be to a different selection threshold. In Figure 2, we assign subhalos into bins of 50 km s^{-1} using v_0 (left) or v_{pk} (right), starting from 50 km s^{-1} (we note that the first bin in either case is incomplete, and the last bin includes all subhalos beyond 250 km s^{-1}). We compare each pair of bins and find that the subhalo counts are only weakly or moderately correlated between bins[7]. This indicates that a halo that is rich in massive subhalos is not necessarily also rich in low-mass subhalos. If the satellite galaxy populations in clusters in different luminosity bins follow the statistical distribution shown here and have such low covariances, they could potentially provide independent information for mass calibration.

3.2. *Scatter of subhalo number*

Boylan-Kolchin et al. (2010) and Busha et al. (2011) have shown that for galactic halos ($M \leq 10^{13.5} h^{-1}\mathrm{M}_\odot$),

[6] To decide the size of the well-resolved ambient region around the main halo, we compare halos in the re-simulated region (composed of high-resolution particles only) with those in the original CARMEN simulation. At 7 h^{-1}Mpc, the re-simulated regions recover the halo population in the corresponding region in the CARMEN simulation. In addition, at 7 h^{-1}Mpc, the number of low-resolution particles is less than 4%, although it varies from halo to halo and is sometimes 0%.

[7] Throughout this work, we use rank correlation, which makes our results insensitive to outliers.

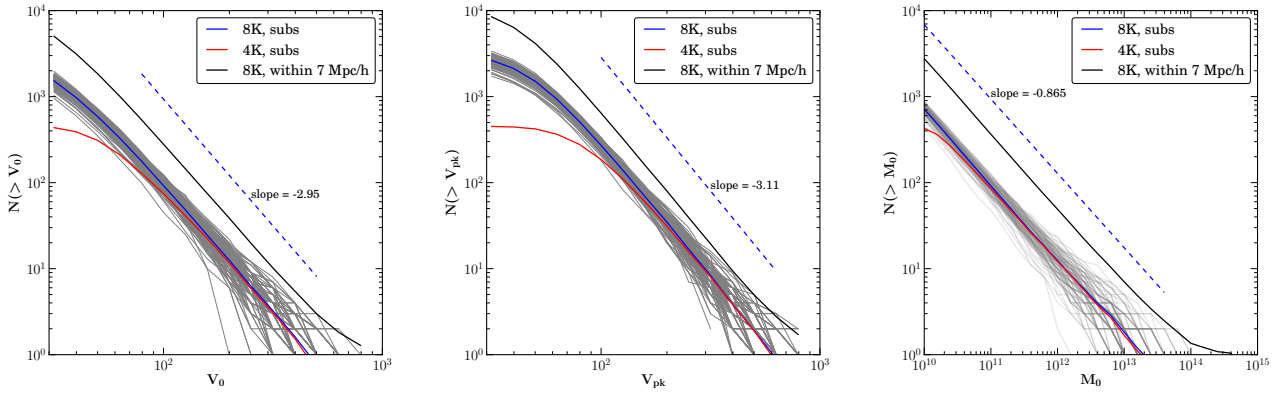

Figure 1. The number of subhalos above a given threshold v_0 (*left*), v_{pk} (*middle*), and M_0 (*right*). The blue/red curves represent the mean number of subhalos within the R_{vir} of RHAPSODY 8K/4K halos, while the black curves represent all halos and subhalos within 7 h^{-1}Mpc around the center of the main halo in the re-simulation. The thin gray curves in the background show the subhalos for individual RHAPSODY 8K halos. The blue dashed line indicates the slope of the 8K sample in the regime where the subhalo sample is complete.

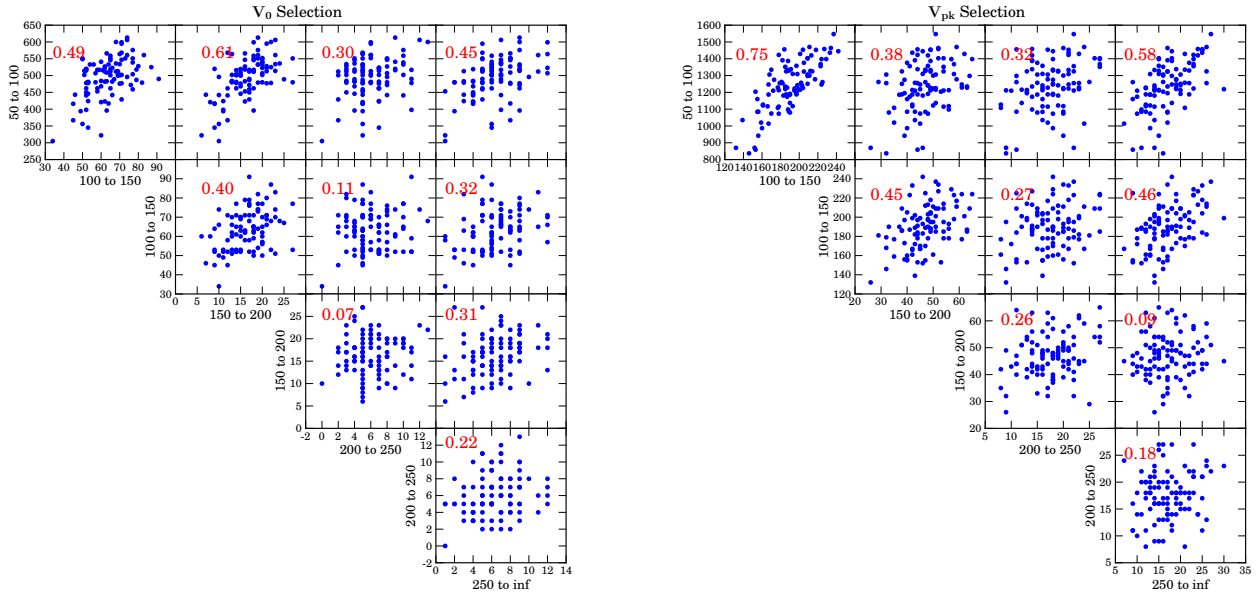

Figure 2. Correlation between the number of subhalos in different bins. Subhalos are binned by v_0 (*left*) or v_{pk} (*right*), with bin size 50 km s^{-1}, starting from 50 km s^{-1}. The subhalo numbers between different bins have moderate or weak correlation.

the distribution function of the number of subhalos (N) deviates from the Poisson distribution when $\langle N\rangle$ is large. We repeat this analysis for our sample of halos of significantly higher mass. Figure 3 shows the scatter of N under different subhalo selection methods and thresholds. The left panel shows the ratio between the measured scatter in the sample $\sigma = \sqrt{\mathrm{Var[N]}}$ and the Poisson scatter $\sigma_{\rm Poisson} = \sqrt{\langle N\rangle}$. The right panel presents the second moment of the subhalo number distribution

$$\alpha = \frac{\sqrt{\langle N(N-1)\rangle}}{\langle N\rangle} \ (\alpha = 1 \text{ for Poisson}) \ . \qquad (2)$$

Both quantities are measures of how the distribution deviates from the Poisson distribution.

In both panels, the x-axis corresponds to $\langle N\rangle$ for a given selection threshold, allowing direct comparison between different subhalo selections. Each curve corresponds to a different selection method, and several corresponding thresholds are marked on each curve (in units of km s^{-1} for maximum circular velocity and $\log_{10} h^{-1}\mathrm{M}_\odot$ for mass). For low thresholds or high $\langle N\rangle$, the scatter deviates significantly from the Poisson scatter. In addition, α has a trend similar to that of $\sigma/\sigma_{\rm Poisson}$ and only slightly deviates from unity. As discussed in Boylan-Kolchin et al. (2010), slight deviations of α from unity can correspond to large deviations from the Poisson distribution. We also note that the additive boost of the variance has a similar trend as α, since $(\sigma^2 - \langle N\rangle)/\langle N\rangle^2 = \alpha^2 - 1$.

From Figure 3, our results for different selection criteria can be summarized as follows:

- v_0 vs. v_{pk} (red vs. blue): v_{pk} selection gives less scatter and is closer to the Poisson distribution,

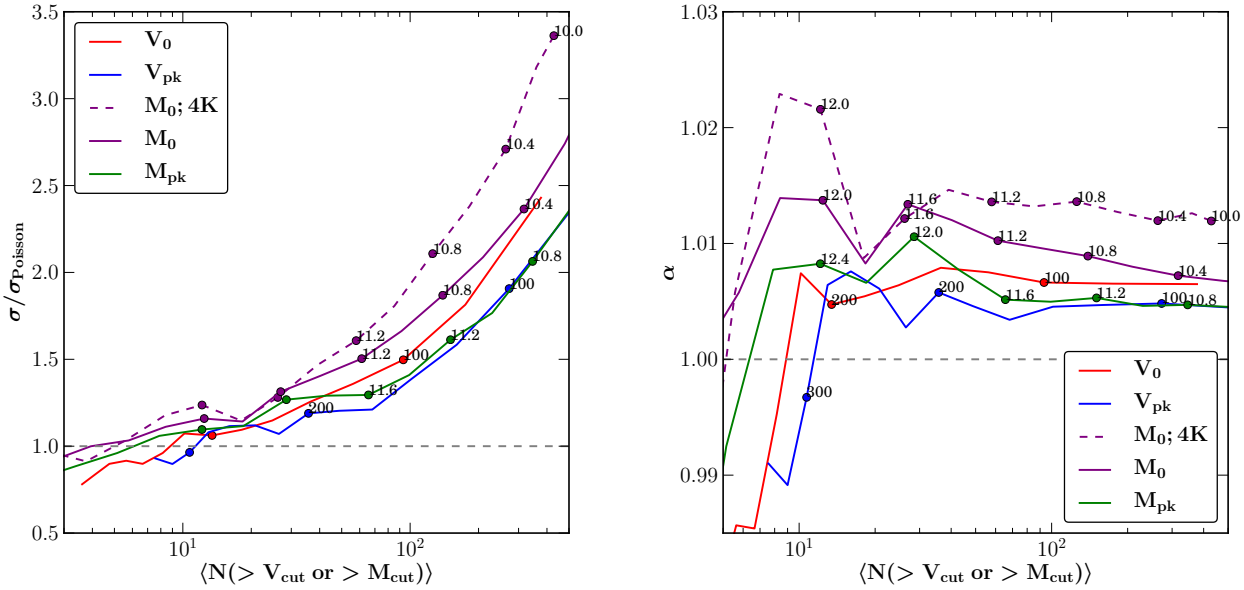

Figure 3. Scatter of the number of subhalos for various selection methods. The left panel corresponds to the ratio between the sample scatter and the Poisson scatter, while the right panel corresponds to the second moment of the distribution. The x-axis is the mean number of subhalos for each selection method, and several of the thresholds are marked on each curve. Here we compare various cases: (1) v_0 vs. v_{pk} (red vs. blue), (2) M_0 vs. M_{pk} (purple vs. green), (3) 4k vs. 8K (purple dashed vs. purple solid). In each pair, the former selection method leads to extra non-Poisson scatter. This trend indicates that both stripping of subhalos and insufficient resolution can induce extra non-Poisson scatter and might lead to a scatter greater than the values in observations. For v_{pk} selection, $\alpha = 1.005$ for sufficiently large $\langle N\rangle$.

indicating that stripping of subhalos can introduce extra non-Poisson scatter.

- M_0 vs. M_{pk} (purple vs. green): M_{pk} selection is closer to the Poisson distribution, which can also be understood with stripping.

- v_{pk} vs. M_{pk} (blue vs. green): similar. Both properties are computed before a subhalo's infall and behave similarly.

- M_0 4K vs. 8K (purple dashed vs. purple solid): 8K is closer to the Poisson distribution, indicating that insufficient resolution can introduce extra non-Poisson scatter.

In all cases presented here, the v_{pk} selection provides the smallest non-Poisson scatter, with an asymptotic value of $\alpha = 1.005$ for sufficiently large $\langle N\rangle$. Our results show that stripping and insufficient resolution can lead to extra non-Poisson scatter. This trend can also explain the modest difference between our values of non-Poisson scatter and those quoted in Boylan-Kolchin et al. (2010), who have higher resolution but used subhalo mass.

3.3. *Subhalo spatial distribution and kinematics*

In Paper I, we have discussed the shape and velocity ellipsoid of dark matter particles of the main halo. It is interesting to see how closely the subhalos follow the distribution of dark matter in position and velocity space, where differences exist, and how these depend on the specific selection of subhalos. We thus present analogous measurements for subhalos, which are selected with v_0 and v_{pk}.

The shape parameters are defined through the distribution tensor:

$$I_{ij} = \langle (r_i - \langle r_i\rangle)(r_j - \langle r_j\rangle)\rangle \ , \tag{3}$$

where r_i is the i^{th} component of the position vector r of a subhalo. The eigenvalues of I_{ij} are sorted as $\lambda_1 > \lambda_2 > \lambda_3$, and the shape parameters are defined as: $a = \sqrt{\lambda_1}$, $b = \sqrt{\lambda_2}$, $c = \sqrt{\lambda_3}$. We present the dimensionless ratios b/a and c/a. In addition, the triaxiality parameter is defined as

$$T = \frac{a^2 - b^2}{a^2 - c^2} \ . \tag{4}$$

$T \approx 1$ ($a > b \approx c$) indicates a *prolate* halo, while $T \approx 0$ ($a \approx b > c$) indicates an *oblate* halo. Intermediate values of T correspond to triaxial halos.

Analogously, the velocity ellipsoid is defined as (e.g., White et al. 2010):

$$\sigma^2_{ij} = \langle (v_i - \langle v_i\rangle)(v_j - \langle v_j\rangle)\rangle \ , \tag{5}$$

where v_i is the i^{th} component of the velocity vector. Sorting the eigenvalues of the velocity ellipsoid as $\lambda_1 > \lambda_2 > \lambda_3$, one can again define $a^{(v)} = \sqrt{\lambda_1}$, $b^{(v)} = \sqrt{\lambda_2}$, $c^{(v)} = \sqrt{\lambda_3}$.

The scatter of the velocity dispersion along different lines of sight can be calculated from the eigenvalues of the velocity ellipsoid tensor as

$$\langle \sigma^2_{los}\rangle = \frac{1}{3}(\lambda_1 + \lambda_2 + \lambda_3) \tag{6}$$

$$(\delta\sigma^2_{los})^2 = \frac{4}{45}(\lambda_1^2 + \lambda_2^2 + \lambda_3^2 - \lambda_1\lambda_2 - \lambda_2\lambda_3 - \lambda_3\lambda_1) \ . \tag{7}$$

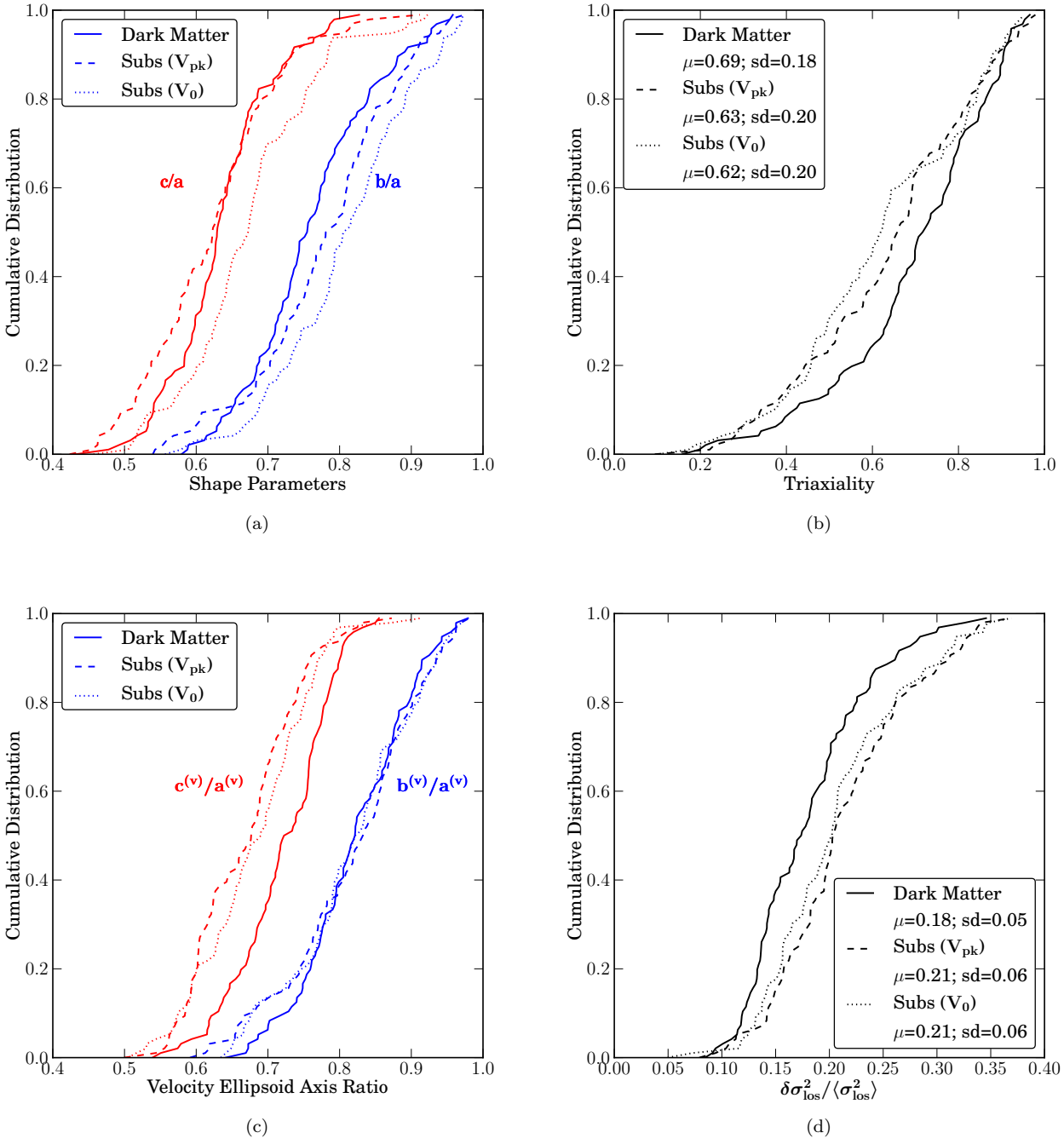

Figure 4. The distribution of the shape and velocity ellipsoid parameters for dark matter particles and subhalos within $R_{\rm vir}$ of the main halos. The upper panels correspond to the shapes of spatial distribution, and the lower panels correspond to the shapes of velocity ellipsoid. As shown in Panels (a) and (b), dark matter particles tend to be more prolate than subhalos. Panel (c) shows that the velocity ellipsoids of subhalos tend to be more elongated. Panel (d) shows that the statistical error of line-of-sight velocity dispersion measurements is larger for subhalos than for dark matter particles.

We use subhalos within $R_{\rm vir}$ selected above a given threshold without imposing weighting.

Figure 4 shows the cumulative distribution function of the shape and velocity ellipsoid parameters of dark matter particles (solid), as well as of subhalos selected with $v_0 > 100$ km s^{-1} (dotted) and subhalos selected with $v_{\rm pk} > 150$ km s^{-1} (dashed). The upper panels show the axis ratios and triaxiality parameters. Subhalos selected by v_0 have a distribution closer to spherical than both $v_{\rm pk}$-selected subhalos and dark matter particles. In addition, the dark matter distribution tends to be more prolate than the subhalo distribution.

The lower panels of Figure 4 show the shape parameters of the velocity ellipsoid and the line-of-sight scatter of the velocity dispersions. We find that the velocities of subhalos tend to be more anisotropic than those of the dark matter particles (based on $c^{(v)}/a^{(v)}$). In addition, $\delta\sigma^2_{los}$ is higher for subhalos than for dark matter particles. This trend can be understood based on the findings of White et al. (2010): the motions of subhalos tend to be anisotropic because they can retain their infall velocities for a long time. In contrast, the merged and stripped material is dynamically older and contributes to a well-mixed isotropic velocity distribution.

We summarize several trends in Figure 4 and propose explanations:

- The distribution of subhalos tends to be more spherical than that of dark matter. This can be understood by the fact that subhalos have a shorter relaxation time than dark matter particles, because $t_{relax} \approx (R/v)(N/\ln N)$ and the N for subhalos is much smaller.
- The velocity ellipsoid of subhalos tends to be more elliptical than that of dark matter. This can be explained by the anisotropic motions of subhalos accreted as a group (as discussed above).
- Subhalos selected with v_0 tend to have a more spherical distribution than those selected with $v_{\rm pk}$. Similar trend exists for $c^{(v)}/a^{(v)}$ but does not exist for $b^{(v)}/a^{(v)}$. This trend can be understood through stripping: a $v_{\rm pk}$ selection tends to include more highly-stripped subhalos than v_0, and highly-stripped subhalos tend to be on more elliptical orbits (stripping will be stronger for those orbits that have a smaller pericenter), leading to the higher ellipticity measured with $v_{\rm pk}$. In addition, we note that overmerging will also make the distribution of subhalos more spherical, because overmerging tends to eliminate highly-stripped subhalos, which tend to have more elliptical orbits (again due to the smaller pericentric distance).

We note that for both v_0 and $v_{\rm pk}$ selection, when we increase the threshold, the ellipticity slightly increases. This trend can be explained by the statistical biases arising when a smaller number of subhalos is used to measure the ellipsoids. To confirm this, we randomly select a number of subhalos within $R_{\rm vir}$ with $\langle N\rangle$ matching either the number of subhalos obtained with the v_0- or $v_{\rm pk}$-selection, and we recover the trend that a smaller number of subhalos always leads to a higher inferred ellipticity. Although it is possible that large radius is weighted more in the position tensor and that small radius is weighted more in the velocity tensor, we find that the radial distribution of massive subhalos alone is insufficient to explain the trend with selection threshold.

In addition, we observe that the difference between shapes measured by dark matter particles and subhalos has a slight trend with the formation history — for halos that experienced recent major mergers, the subhalo distribution tends to be much rounder than the total dark matter particle distribution. This could also be related to the fact that subhalos have a shorter relaxation time than dark matter particles.

Finally, we note that in all cases, the differences in axis ratios are at the level of a few percent. Observationally, these differences are likely to be overwhelmed by the scatter due to line-of-sight projection, viewing angle, spectroscopic sample selection, etc. These effects are likely to depend on the environment and details of the observational techniques employed. It would be interesting to investigate whether and, if so, how the difference between the velocity ellipsoids for the various selection criteria depends on environment (see also Faltenbacher 2010, who have demonstrated a dependence of subhalo kinematics on environment in the Millennium Simulation). An analysis of the environmental dependence of halo properties will be deferred to a future paper.

4. CORRELATION BETWEEN SUBHALO PROPERTIES AND FORMATION HISTORY

In Paper I, we have focused on the impact of the formation history on the density profile and the phase-space structure of the cluster halos. Here, we investigate the impact of the formation history on the subhalo population. In Figure 5, we present the correlation of eight quantities measured from our sample: four for subhalo properties, three for formation time, and one for the halo profile.

4.1. *Formation history parameters*

As discussed in Paper I, to quantify the formation history of halos, we adopt an exponential-plus-power law model with two parameters (McBride et al. 2009)

$$M(z) = M_0(1+z)^{\beta}e^{-\gamma z}\ , \tag{8}$$

$$-\frac{d\ln M}{dz} \approx \gamma - \beta \ \ \text{when } z << 1\ . \tag{9}$$

Thus, $\gamma - \beta$ provides a measure of the late-time accretion rate.

We use $z_{1/2}$, the earliest redshift that a halo obtains half of its mass, as the formation time proxy throughout the paper, but note that using formation time proxies based on fitting functions (as those studied in Paper I) lead to similar results. In addition, we include the redshift of the last major merger of each main halo, z_{lmm}.

We note that the formation history is directly reflected in the halo density profile, which has been studied in detail in Paper I. For the completeness of our correlation analysis, we also include the halo concentration defined for the Navarro–Frenk–White (NFW) profile (Navarro et al. 1997):

$$\frac{\rho(r)}{\rho_{crit}} = \frac{\delta_c}{(r/r_s)(1+r/r_s)^2}\ , \tag{10}$$

for which the concentration parameter is defined as

$$c_{\rm NFW} = \frac{R_{\rm vir}}{r_s} \ . \tag{11}$$

We kindly refer the reader to Paper I for details on the fitting procedure.

4.2. *Subhalo mass fraction*

We next investigate the mass of the main halos that is contained in subhalos. The subhalo mass fraction can be defined as

$$f_{sub}(M_{th}) = \frac{1}{M_{main}} \sum_{M_{sub}>M_{th}} M_{sub} \tag{12}$$

and can be used as an indication of a recent major merger event. For example, if a massive subhalo accreted onto the main halo only recently, it retains most of its mass and contributes to a large f_{sub}. We show below that f_{sub} is correlated with halo formation time and can thus be used as an indicator of the state of relaxedness of the halo (e.g., De Lucia et al. 2004; Shaw et al. 2006). Here we choose $M_{th} = 10^{10}h^{-1}{\rm M}_{\odot}$, which approximately corresponds to our completeness limit (see Fig. 1), but note that the correlations presented below are insensitive to the specific choice of M_{th}.

The third row and column of Figure 5 correspond to f_{sub} and show, as expected, that f_{sub} is strongly correlated with $z_{1/2}$, $\gamma - \beta$, and $c_{\rm NFW}$. That is, halos of higher f_{sub} tend to be late-forming, with high late-time accretion rates and associated low concentration.

The subhalo mass fraction itself is also a quantity of observational interest. For example, it can be inferred from gravitational lensing (e.g., Dalal & Kochanek 2002; Vegetti et al. 2012; Fadely & Keeton 2012). Accurate modeling of the subhalo mass fraction is essential for the study of the lensing flux ratios (e.g., Xu et al. 2009). For the relatively massive systems considered here, we find that f_{sub} is strongly correlated with the mass of the most massive subhalo, despite the fact that this halo contributes on average only $\sim 20\%$ of the total subhalo fraction. We also find that the subhalo fraction is strongly correlated with the dominance of the main halo (related to the luminosity gap between brightest and second brightest galaxies), as well as with formation time and concentration. Because strong lensing clusters tend to have higher than average halo concentrations, it is important to take this correlation into account when interpreting measurements of the subhalo mass fraction from strong lensing.

4.3. *Mass contributed by merged subhalos*

In the previous subsection, we addressed the mass contributed by the *present* subhalo population. We now investigate the mass that was brought into the main halo by all merging events in a halo's history. Figure 6 shows the contribution to the main halo mass from merged subhalos. This has also been explored by, e.g., Berrier et al. (2009) for lower mass systems. The x-axis corresponds to the ratio of subhalo mass to main halo mass, $\mu = M^{sub}/M_0^{main}$, and the y-axis corresponds to the fraction of main halo mass contributed by subhalos above a given μ.

Here we consider two types of subhalos. The *first type* is those subhalos that have merged into the main halo and can no longer be identified; for this type of subhalo, we use its mass when it accreted onto the main halo, $M_{\rm ac}$. These subhalos are represented by the blue curve, and the blue shaded region corresponds to its standard deviation. Our results indicate that, on average, 60% of the main halo's mass comes from merged subhalos with $\mu > 10^{-4}$; however, this number varies greatly from halo to halo.

The *second type* is those subhalos that still survive today (i.e., that can be identified by the halo finder at $z = 0$). For this type, we also use $M_{\rm ac}$. Since subhalos tend to lose a significant amount of mass due to tidal stripping inside the main halos, using $M_{\rm ac}$ ensures that we include the mass that once belonged to subhalos but later got stripped by the main halo. We do not explicitly count the subhalos that merge into other subhalos because their masses have already been included in the surviving subhalos. The red curve corresponds to the sum of the first and the second types. We find that more than 90% of the mass can be attributed to halos with $\mu > 10^{-4}$ that were accreted onto the main halo.

Finally, the black curve shows the contribution to main halo from subhalos that survive at $z = 0$. We use the current mass of these subhalos, M_0; this quantity is equivalent to the subhalo mass fraction for different mass thresholds, $f_{sub}(> \mu)$. Subhalos with $\mu > 10^{-4}$ constitute a little less than 20% of the mass of the main halo.

4.4. *Dominance of the main halo*

In this section, we study the difference between each main halo and its largest subhalo, a quantity motivated by the definition of the so-called "fossil groups". Observationally, these systems are defined as having a large magnitude gap between the brightest and second brightest galaxies, in addition to being X-ray luminous (e.g., Tremaine & Richstone 1977; Jones et al. 2003; Miller et al. 2012). Fossil systems are often interpreted as a population of galaxy groups that have assembled at early times and have not undergone a recent major merger.

Since predicting the optical and X-ray properties of our halos is beyond the scope of this paper, we define a related property, the ratio of $\rm v_{pk}$ for the main and the first subhalo (the subhalo with highest $\rm v_{pk}$):

$$D = \frac{\rm v_{pk}^{main}}{\rm v_{pk}^{1st\ sub}}. \tag{13}$$

We note that using the second subhalo leads to the same trend presented below.

In Figure 5, the fourth column and row show that D is correlated with the formation time, late-time accretion, concentration, and subhalo mass fraction. We also note that all our main halos have similar $\rm v_{pk}^{main}$; therefore, the scatter in D is almost completely determined by $\rm v_{pk}^{1st\ sub}$.

The trends observed in Figure 5 can be understood as follows: Since $\rm v_{pk}^{1st\ sub}$ indicates the maximum of the subhalo mass that accretes onto a main halo, a main halo with a low $\rm v_{pk}^{1st\ sub}$ has fewer massive subhalos accreting onto it (this is also reflected by its low f_{sub}). With relatively fewer incoming subhalos, to achieve the same mass today, these halos must have obtained most of their mass at early times and have undergone slow accretion at late time, thus leading to the low $\gamma - \beta$ and the high concentration.

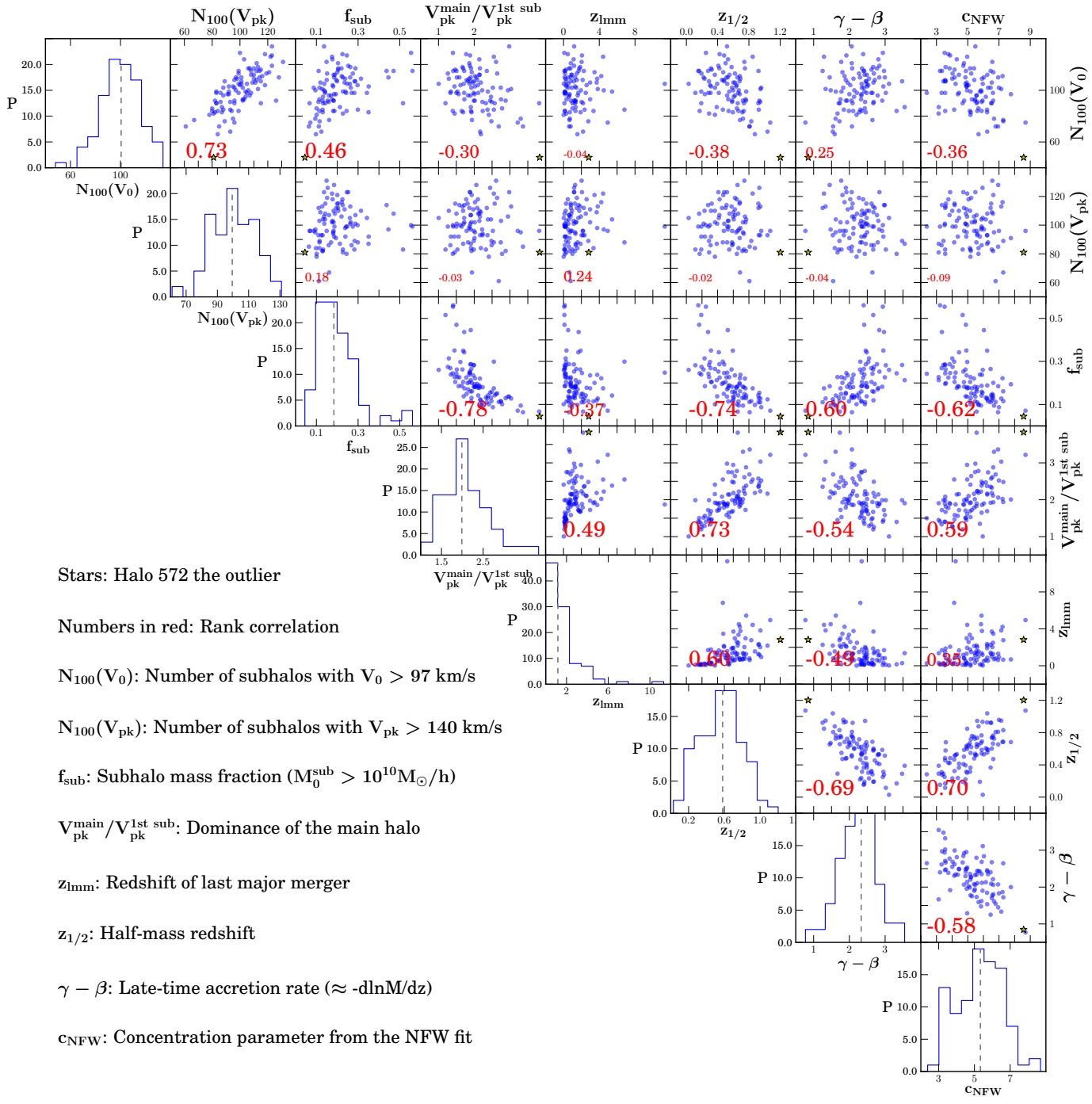

Figure 5. Correlation between the subhalo properties and the formation time proxies. The top two rows show the number of subhalos selected with v_0 and v_{pk}. In each case, the threshold is chosen to have an average of 100 subhalos per main halo. Correlations tend to be weaker with subhalos selected by v_{pk} than by v_0, except for z_{lmm}.

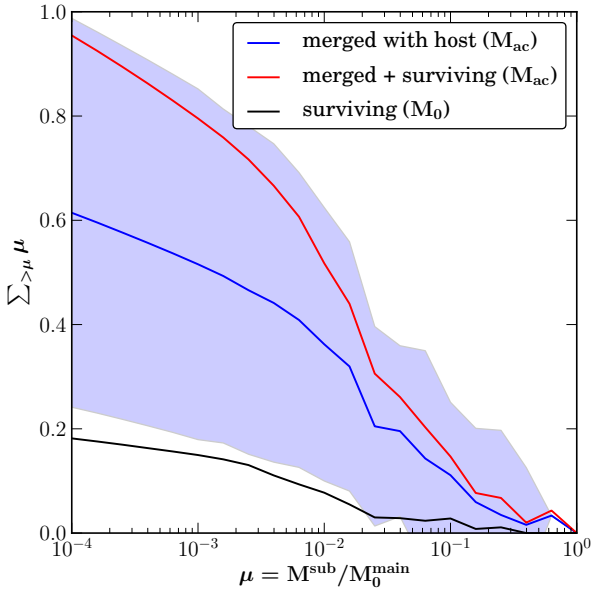

Figure 6. The contribution of mass to the main halo from subhalos above a certain mass ratio $\mu = M^{sub}/M_0^{main}$. The blue curve corresponds to the contribution from subhalos that have merged with the main halo, and we use the subhalo mass at accretion, $M_{\rm ac}$; the shaded area corresponds to the standard deviation of the sample. The red curve includes merged subhalos and those that are surviving, for which we also use $M_{\rm ac}$. The black curve corresponds to subhalos that are still surviving today, for which M_0 is used, and is equivalent to $f_{sub}(>\mu)$.

While we were preparing this manuscript, we learned about the related work of Hearin et al. (2012), who have studied the "magnitude gap" of the two brightest cluster members, which is analogous to our dominance parameter D. These authors have found that for SDSS groups of a given velocity dispersion, clusters with high magnitude gap tend to have low richness, and this correlation can in turn reduce the scatter in the mass inferences using optical mass tracers. In contrast, we find that the number of subhalos selected with $v_{\rm pk}$ is not correlated with D for halos of the same mass. Since the results from Hearin et al. (2012) are based on velocity dispersion rather than mass, a fair comparison between our results and theirs will require further consideration of the scatter in velocity dispersion, scatter of galaxy luminosity at a given $v_{\rm pk}$, as well as observational selections, which are beyond the scope of the current work.

4.5. *The curious case of Halo 572: An outlier and a fossil cluster*

In the RHAPSODY sample, we find one peculiar halo—Halo 572—which is a prominent outlier in formation time (highest $z_{1/2}$) and occupies the tail of many halo properties as well as the corner of several scatter plots (marked as stars in Figure 5). It has unusually high $c_{\rm NFW}$ (2.7σ deviation from the mean) and central dominance (3.2σ). It also has one of the lowest late-time accretion rates $\gamma - \beta$ (2.7σ), f_{sub} (1.6σ), and subhalo numbers selected with several different criteria. This halo obtained most of its mass at early time and nearly stopped accreting mass at late time, leading to these extreme properties. Images of the evolution of Halo 572 are shown in Figure 3 of Paper I, where it is evident that this halo had an atypical formation history. We find that Halo 572 does *not* live in an atypical environment on large scales.

The high central dominance indicates that, if such a halo is observed, it would likely have a large luminosity gap between the brightest and second brightest galaxies, and its high concentration will make it X-ray luminous. Therefore, we expect that this halo will host a cluster that satisfies the criteria of a "fossil." In addition, it is a "real" fossil cluster in the sense that it has an unusually early formation history. Studies of fossil groups in both simulations and observations have come to a range of conclusions, with debate about whether fossil groups have distinct assembly histories or are merely an intermediate state in galaxy formation (see, e.g., Cui et al. 2011; Sales et al. 2007; and references therein). Halo 572 presents a case of a distinctively early formation history and the consequential properties. From these results we conclude that it is highly probable that "real fossils" exist in the universe but that they are very rare; thus, they require more stringent selection criteria to be distinguished from some transient states of cluster formation.

5. CORRELATION BETWEEN FORMATION TIME AND SUBHALO NUMBER: THE IMPACT OF SUBHALO SELECTION

In this section, we investigate in detail the correlation between formation time and subhalo abundance (as previously explored by e.g., Zentner et al. 2005; Wechsler et al. 2006; Giocoli et al. 2010). We show that this correlation is mainly caused by subhalo stripping and insufficient resolution. However, in the real universe, stripping of dark matter particles is less relevant to the galaxy content in clusters, and this correlation is therefore not expected to exist for observable galaxies.

Zentner et al. (2005) found that early-forming halos tend to have fewer subhalos. In their study, subhalos are selected with a threshold on v_0 ($v_{\rm max}$ at $z = 0$). This trend has been explained by the fact that in early-forming halos, subhalos tend to accrete at early time and are more likely to be destroyed, which leads to a low number of subhalos. However, we find that this correlation strongly depends on how subhalos are selected. In what follows, we explore the dependence of this correlation on various subhalo selection criteria and understand the trend by investigating the accretion and stripping of subhalos.

Figure 7 demonstrates how subhalo selection based on v_0 or $v_{\rm pk}$ can lead to different correlations between formation time and subhalo number. The left panel corresponds to selecting subhalos with $v_0 > 100$ km s^{-1}, and the right panel corresponds to $v_{\rm pk} > 150$ km s^{-1}. We note these two thresholds correspond to roughly the same number of subhalos. Each point corresponds to a main halo in our sample. The x-axes correspond to the number of subhalos under either selection criterion, and the y-axes correspond to the formation time proxy $z_{1/2}$. When subhalos are selected based on v_0 (left panel), formation time and subhalo number are significantly anti-correlated. However, when subhalos are selected based on $v_{\rm pk}$ (right panel), this anti-correlation no longer exists in our sample.

This lack of anti-correlation can be understood as follows. When subhalos are selected with a given threshold of v_0, the stripping of subhalos directly impacts the subhalo

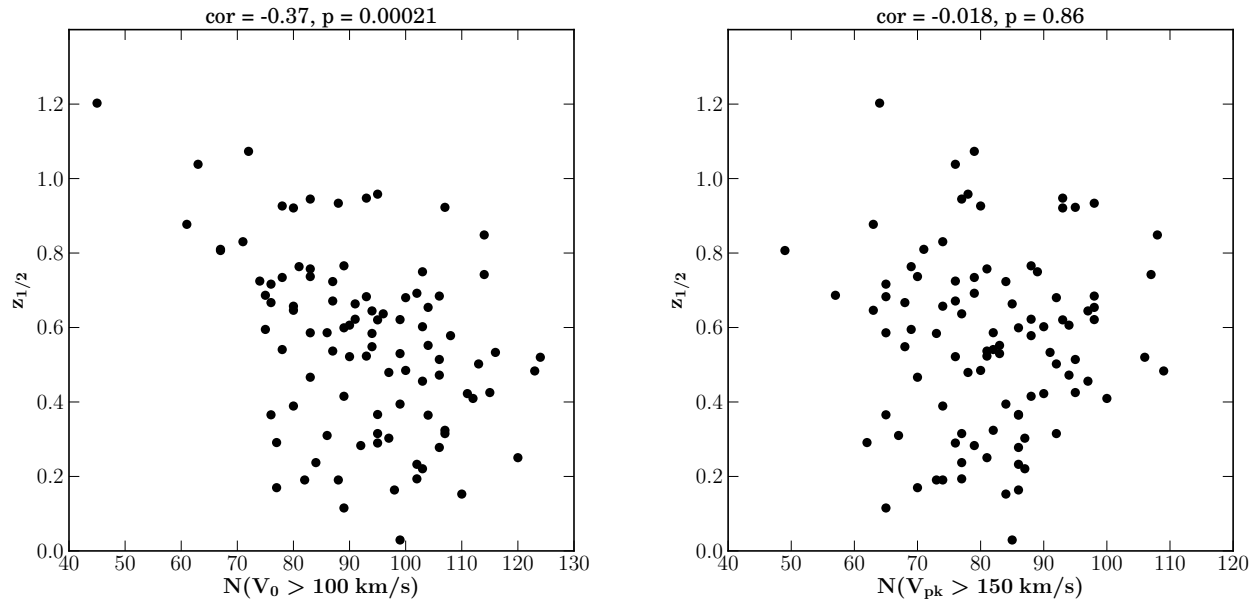

Figure 7. The impact of subhalo selection on the correlation between subhalo number and formation time $z_{1/2}$. The left panel corresponds to selecting subhalos using $v_0 > 100$ km s^{-1}, while the right panel corresponds to $v_{pk} > 150$ km s^{-1}. Although the v_0 selection presents significant anti-correlation between subhalo number and formation time, the v_{pk} selection presents no such correlation. This trend can be explained by the stripping of subhalos, as demonstrated by the following two figures.

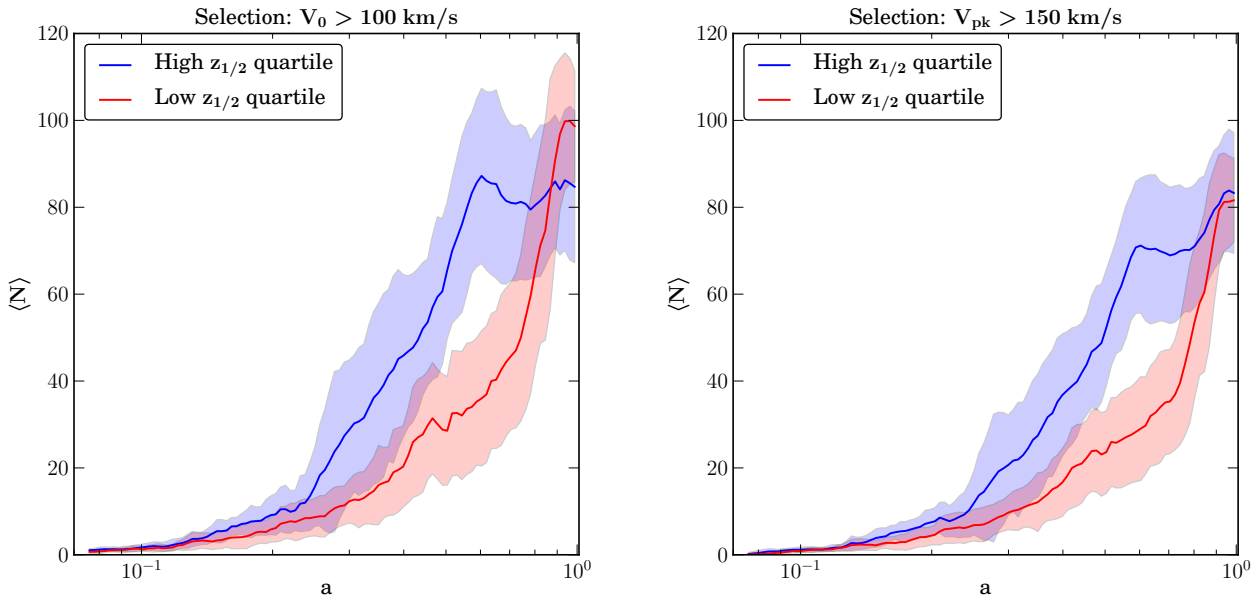

Figure 8. The evolution of subhalo number, split by quartiles of $z_{1/2}$. *Left:* subhalos with $v_0 > 100$ km s^{-1}; *right:* subhalos with $v_{pk} > 150$km s^{-1}. When subhalos are selected with v_0, the subhalo number of early-forming (blue) and late-forming (red) halos split at $z = 0$; however, when subhalos are selected with v_{pk}, there is no clear split of halo number at $z = 0$. This trend is reflected by the difference in the correlation seen in Figure 7.

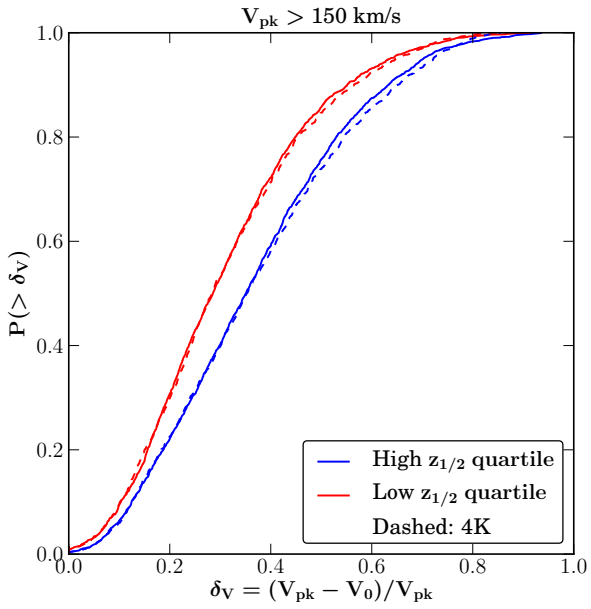

Figure 9. Cumulative distribution function of $\delta_{v_{max}} = (v_{pk} - v_0)/v_{pk}$, an indication of the amount of stripping experienced by subhalos. We split the main halo by the formation time $z_{1/2}$. Early-forming halos (blue) tend to have subhalos with higher $\delta_{v_{max}}$ (stronger stripping) on average than late-forming ones (red). If subhalos are selected with v_0, highly-stripped subhalos tend to fall below the threshold, leading to a low subhalo number. This can explain the correlation seen in the v_0 selection in Figures 7 and 8.

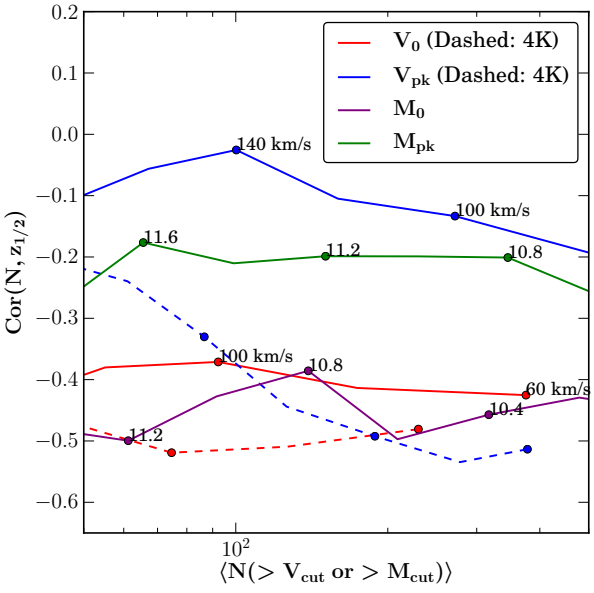

Figure 10. Correlation between subhalo number and $z_{1/2}$, for different subhalo selection methods. When subhalos are selected with v_0 or M_0 (red and purple), an anti-correlation exists for all thresholds; when subhalos are selected with v_{pk} or M_{pk} (blue and green), the anti-correlation is greatly reduced or non-existent. In addition, the comparison between 8K and 4K (solid and dashed of the same color) sample shows that the anti-correlation can be enhanced by insufficient resolution.

number: for a halo that assembled earlier, its subhalos experience stripping for a longer time and with a higher intensity (because of the high halo concentration), and the subhalos' masses and v_0 tend to be greatly reduced. Therefore, fewer subhalos remain above the v_0 threshold. On the other hand, when we select subhalos using v_{pk}, the stripping of subhalos does not directly impact the subhalo number, as long as those subhalos are still identifiable.

To support our argument above, we investigate the evolution of the subhalo population for these two subhalo selection criteria. Figure 8 shows subhalo number as a function of the scale factor a (we plot in $\log a$ to emphasize the late-time behavior). As in the previous figure, the left/right panel corresponds to the v_0/v_{pk} selection. In both panels, we plot the subhalo number evolution for the highest $z_{1/2}$ quartile (blue) and lowest $z_{1/2}$ quartile (red).

In the left panel of Figure 8, we can see that for early-forming halos (blue), the subhalo accretion rate is high at early time but suddenly declines after $a \approx 0.6$. On the other hand, for the late-forming halos (red), their subhalo accretion rate is high at late time. At $a \simeq 1$, the early-forming halos have fewer subhalos than late-forming halos. In the right panel, although the early-forming halos have declined in subhalo accretion rate at late time, their subhalo number still grows at late times, and their subhalo numbers are similar to late-forming halos at $a \simeq 1$.

The different trends in both panels can be attributed primarily to the stripping of subhalos. Figure 9 shows the cumulative distribution of the fractional change of v_{max} of subhalos

$$\delta_{v_{max}} = \frac{v_{pk} - v_0}{v_{pk}} \ . \qquad (14)$$

This quantity can be used as a measure of the amount of stripping experienced by subhalos. Higher $\delta_{v_{max}}$ indicates that a subhalo has experienced stronger or longer stripping and has lost more mass. For early-forming halos (blue), subhalos on average have higher $\delta_{v_{max}}$, indicating that these subhalos experience more stripping and their v_{max} is reduced more. As a result, if we select subhalos using v_0, we tend to exclude subhalos that have experienced more stripping. These subhalos will however be included if we select subhalos using v_0.

Therefore, the correlation between formation time and subhalo number seen in a selection on v_0 can be attributed to the exclusion of highly-stripped subhalos. Since subhalos selected with v_0 have less observational relevance than those selected with v_{pk}, our results imply that cluster richness is unlikely to be correlated with the formation time of the halo in observations.

So far we have been using two specific selection thresholds for v_0 and v_{pk}. Here, we investigate how our results depend on the selection threshold. In Figure 10, we present the correlation between subhalo number and halo formation redshift, $Cor(N, z_{1/2})$, where N is the subhalo number above some selection thresholds. We discuss four selection methods: v_0, v_{pk}, M_0, and M_{pk}. For each selection threshold, we compute the mean number of subhalos, $\langle N \rangle$. Using $\langle N \rangle$ as the x-axis allows us to put these curves on the same figure.

In Figure 10, the different magnitudes of correlation can easily be seen. Here we compare four pairs of selection

methods:

- v_0 vs. v_{pk} (red vs. blue): the former has stronger correlation with $z_{1/2}$ due to subhalo stripping, as discussed above.
- M_0 vs. M_{pk} (purple vs. green): the former has stronger correlation, for the same reason as above.
- v_0 vs. v_0 4K (red solid vs. red dashed): the latter has stronger correlation, indicating that an unphysical correlation can be introduced by insufficient resolution.
- v_{pk} vs. v_{pk} 4K (blue solid vs. blue dashed): the latter has stronger correlation, indicating that using v_{pk} does not mitigate the impact of resolution. For other quantities, comparisons between 8K and 4K show the same trend.

Since v_{pk} is more relevant for observations than v_0, M_0, and M_{pk}, the lack of correlation when selecting by v_{pk} indicates that, observationally, the formation time of a galaxy cluster is unlikely to be inferred from the number of galaxies alone. Thus, richness-selected galaxy clusters are unlikely to be biased in terms of their formation time, implying that the effect of assembly bias may be negligible for cluster cosmology self-calibration (Wu et al. 2008).

We now return to the discussion of Figure 5. We have shown that various observables, including the subhalo fraction, the central dominance, and the concentration, are highly correlated with formation time and the amount of late-time accretion. These observables are also correlated with the number of subhalos selected by the current maximum circular velocity, v_0. However, these correlations largely disappear when selecting subhalos based on v_{pk}, which is expected to be more strongly correlated with galaxy luminosity or stellar mass (Conroy et al. 2006; Reddick et al. 2012). This reduces the likelihood that these observables provide additional mass information for richness-selected samples of galaxy clusters.

6. SUMMARY AND DISCUSSION

In this paper, we have presented the key properties of the subhalo populations in the RHAPSODY cluster re-simulation project, a sample of 96 halos of $M_{vir} = 10^{14.8\pm0.05}h^{-1}M_\odot$, resolved with approximately 5×10^6 particles inside the virial radius. We focus on the effect of formation history on the subhalo population. We find that this effect depends on subhalo selection criteria and resolution, which need to be carefully taken into account to make observationally relevant inferences. Our findings can be summarized as follows:

1. **Subhalo statistics:** In §3.1, we show the subhalo mass function for several subhalo mass proxies: v_0, v_{pk}, and M_0. We find that for a given halo, the numbers of large and small subhalos are only moderately correlated with each other. In §3.2, we compare the scatter in subhalo number under different selection criteria and resolutions, finding that subhalo stripping and insufficient resolution can lead to extra non-Poisson scatter. The least stripped proxy, v_{pk} (8K), still has a small amount of residual scatter above Poisson statistics, corresponding to a constant value of $\alpha = 1.005$.
2. **Shape of spatial distribution and velocity ellipsoid:** In §3.3, we compare these quantities measured from subhalos selected with v_0 and v_{pk}, as well as from dark matter particles. We find that dark matter particles tend to have a more prolate distribution than subhalos, and that subhalos show a higher line-of-sight scatter of velocity dispersion. Subhalos selected with v_{pk} are slightly more elliptically distributed than those selected with v_0.
3. **Formation history and subhalo properties:** We have quantified the correlations between various subhalo properties and halo formation history in §4 and in Figure 5. The fraction of mass in subhalos and the central dominance are both highly correlated with formation time, late-time accretion rate, and concentration. These correlations have important implications for interpreting lensing-selected and X-ray selected clusters.
4. **A fossil cluster:** Our sample includes a peculiar outlier, Halo 572 (presented in §4.5), with exceptionally high formation redshift, concentration, and central dominance. It also has exceptionally low late-time mass accretion rate, subhalo number, and subhalo mass fraction. This finding indicates that halos of distinct formation history are likely to be distinguishable observationally, if stringent selection criteria are used.
5. **Impact of tidal stripping on the occupation number of subhalos:** In §5, we have demonstrated that the subhalo number, when selected using v_{pk} (a more observationally relevant property), does not correlate with formation time. This is in contrast to the result, shown previously and confirmed here, that early-forming halos have fewer subhalos when selected with v_0. We demonstrate that the correlation with the number of subhalos selected with v_0 can be attributed to subhalo stripping and insufficient resolution and is thus largely overestimated for cluster satellite galaxies. This finding implies that the assumption that halo occupation number is independent of formation time at fixed mass is likely to be a good one for luminosity or stellar mass selected samples, and that the formation history of clusters is unlikely to be directly inferred from the number of their satellite galaxies.

In a forthcoming paper (Wu et al., in preparation), we will address the issue of the completeness of subhalo populations in detail by comparing simulations of different resolutions directly with observations. We will also investigate the impact of completeness on the measured velocity dispersion of subhalos.

The lack of a correlation between halo occupation number and formation time provides support for halo occupation models that depend only on halo mass, when the galaxy samples are selected by stellar mass or luminosity. However, our findings indicate that the halo occupation is likely a function of selection; the halo occupation of color-selected samples may depend on formation time. This appears to be consistent with some observational studies; e.g., the luminosity-selected samples studied in Tinker & Conroy (2009) did not show evidence for trends

with formation time, while evidence for this dependence in samples selected by star formation rate was presented by Tinker et al. (2012).

Although we have found that the formation history of clusters does not manifest itself in the number of galaxies, correlation with formation time still exists for subhalo mass fraction, central dominance, and halo concentration. These correlations are potentially observable in targeted lensing programs like CLASH (Postman et al. 2011), optical follow-up programs for clusters detected by the South Pole Telescope (High et al. 2012; Song et al. 2012), as well as the recent lensing mass calibration for X-ray selected clusters by von der Linden et al. (2012). These properties together can indicate a system's state of relaxedness and can potentially be combined to reduce the scatter in the observable–mass relation for multi-wavelength surveys.

Finally, the dependence of subhalo statistics on the selection method could potentially impact the prediction of galaxy clustering based on the halo model. For example, it is common to assume that the galaxy number is described by a Poisson distribution, or that their spatial distribution and velocities follow those of the dark matter particles (e.g., Zehavi et al. 2011; Cacciato et al. 2012). As we have shown, these assumptions depend on the specific subhalo selection applied and on the simulation resolution and are still uncertain. Therefore, these uncertainties will potentially limit the accuracy with which we can predict the small-scale clustering and hence our ability to use it to infer cosmological parameters.

We thank Gus Evrard, Eduardo Rozo, Michael Busha, Matt Becker, and Andrew Wetzel for many helpful suggestions and comments. We are grateful to Michael Busha for providing the Carmen simulation on which the Rhapsody sample was based. This work was supported by the U.S. Department of Energy under contract numbers DE-AC02-76SF00515 and DE-FG02-95ER40899, and by Stanford University through a Gabilan Stanford Graduate Fellowship to HW and a Terman Fellowship to RHW. Additional support was provided by SLAC-LDRD-0030-12.

REFERENCES

Allen, S. W., Evrard, A. E., & Mantz, A. B. 2011, ARA&A, 49, 409
Angulo, R. E., Lacey, C. G., Baugh, C. M., & Frenk, C. S. 2009, MNRAS, 399, 983
Behroozi, P. S., Wechsler, R. H., & Wu, H.-Y. 2011a, arXiv:1110.4372
Behroozi, P. S., Wechsler, R. H., Wu, H.-Y., Busha, M. T., Klypin, A. A., & Primack, J. R. 2011b, arXiv:1110.4370
Berrier, J. C., Stewart, K. R., Bullock, J. S., Purcell, C. W., Barton, E. J., & Wechsler, R. H. 2009, ApJ, 690, 1292
Boylan-Kolchin, M., Springel, V., White, S. D. M., & Jenkins, A. 2010, MNRAS, 406, 896
Bryan, G. L. & Norman, M. L. 1998, ApJ, 495, 80
Busha, M. T., Wechsler, R. H., Behroozi, P. S., Gerke, B. F., Klypin, A. A., & Primack, J. R. 2011, ApJ, 743, 117
Cacciato, M., van den Bosch, F. C., More, S., Mo, H., & Yang, X. 2012, arXiv:1207.0503
Cohn, J. D., Evrard, A. E., White, M., Croton, D., & Ellingson, E. 2007, MNRAS, 382, 1738
Conroy, C., Wechsler, R. H., & Kravtsov, A. V. 2006, ApJ, 647, 201
Cui, W., Springel, V., Yang, X., De Lucia, G., & Borgani, S. 2011, MNRAS, 416, 2997
Dalal, N. & Kochanek, C. S. 2002, ApJ, 572, 25
De Lucia, G. et al. 2004, MNRAS, 348, 333
Erickson, B. M. S., Cunha, C. E., & Evrard, A. E. 2011, Phys. Rev. D, 84, 103506
Fadely, R. & Keeton, C. R. 2012, MNRAS, 419, 936
Faltenbacher, A. 2010, MNRAS, 408, 1113
Gao, L., De Lucia, G., White, S. D. M., & Jenkins, A. 2004, MNRAS, 352, L1
Gao, L., Navarro, J. F., Frenk, C. S., Jenkins, A., Springel, V., & White, S. D. M. 2012, arXiv:1201.1940
Ghigna, S., Moore, B., Governato, F., Lake, G., Quinn, T., & Stadel, J. 1998, MNRAS, 300, 146
Giocoli, C., Tormen, G., Sheth, R. K., & van den Bosch, F. C. 2010, MNRAS, 404, 502
Hahn, O. & Abel, T. 2011, MNRAS, 415, 2101
Hearin, A. P., Zentner, A. R., Newman, J. A., & Berlind, A. A. 2012, arXiv:1207.1074
High, F. W. et al. 2012, arXiv:1205.3103
Jones, L. R., Ponman, T. J., Horton, A., Babul, A., Ebeling, H., & Burke, D. J. 2003, MNRAS, 343, 627
Klypin, A., Gottlöber, S., Kravtsov, A. V., & Khokhlov, A. M. 1999, ApJ, 516, 530
Kravtsov, A. V., Berlind, A. A., Wechsler, R. H., Klypin, A. A., Gottlöber, S., Allgood, B., & Primack, J. R. 2004, ApJ, 609, 35
McBride, J., Fakhouri, O., & Ma, C.-P. 2009, MNRAS, 398, 1858
Miller, E. D. et al. 2012, ApJ, 747, 94
Moore, B., Ghigna, S., Governato, F., Lake, G., Quinn, T., Stadel, J., & Tozzi, P. 1999, ApJ, 524, L19
Moore, B., Governato, F., Quinn, T., Stadel, J., & Lake, G. 1998, ApJ, 499, L5
Nagai, D. & Kravtsov, A. V. 2005, ApJ, 618, 557
Navarro, J. F., Frenk, C. S., & White, S. D. M. 1997, ApJ, 490, 493
Onions, J. et al. 2012, MNRAS, 423, 1200
Postman, M. et al. 2011, arXiv:1106.3328
Purcell, C. W. & Zentner, A. R. 2012, arXiv:1208.4602
Reddick, R. M., Wechsler, R. H., Tinker, J. L., & Behroozi, P. S. 2012, arXiv:1207.2160
Rozo, E., Bartlett, J. G., Evrard, A. E., & Rykoff, E. S. 2012, arXiv:1204.6305
Rozo, E., Rykoff, E., Koester, B., Nord, B., Wu, H.-Y., Evrard, A., & Wechsler, R. 2011, arXiv:1104.2090
Rozo, E. et al. 2009, ApJ, 703, 601
Rykoff, E. S. et al. 2012, ApJ, 746, 178
Sales, L. V., Navarro, J. F., Lambas, D. G., White, S. D. M., & Croton, D. J. 2007, MNRAS, 382, 1901
Shaw, L. D., Weller, J., Ostriker, J. P., & Bode, P. 2006, ApJ, 646, 815
Song, J. et al. 2012, arXiv:1207.4369
Springel, V. 2005, MNRAS, 364, 1105
Tinker, J. L. & Conroy, C. 2009, ApJ, 691, 633
Tinker, J. L. et al. 2012, ApJ, 755, L5
Tremaine, S. D. & Richstone, D. O. 1977, ApJ, 212, 311
Vegetti, S., Lagattuta, D. J., McKean, J. P., Auger, M. W., Fassnacht, C. D., & Koopmans, L. V. E. 2012, Nature, 481, 341
von der Linden, A. et al. 2012, arXiv:1208.0597
Wang, J., Frenk, C. S., Navarro, J. F., & Gao, L. 2012, arXiv:1203.4097
Wechsler, R. H., Zentner, A. R., Bullock, J. S., Kravtsov, A. V., & Allgood, B. 2006, ApJ, 652, 71
Weinberg, D. H., Mortonson, M. J., Eisenstein, D. J., Hirata, C., Riess, A. G., & Rozo, E. 2012, arXiv:1201.2434
Wetzel, A. R., Tinker, J. L., Conroy, C., & van den Bosch, F. C. 2012, arXiv:1206.3571
White, M., Cohn, J. D., & Smit, R. 2010, MNRAS, 1221
Wu, H.-Y., Hahn, O., Wechsler, R. H., Mao, Y.-Y., & Behroozi, P. S. 2012, arXiv:1209.3309
Wu, H.-Y., Rozo, E., & Wechsler, R. H. 2008, ApJ, 688, 729
Wu, H.-Y., Zentner, A. R., & Wechsler, R. H. 2010, ApJ, 713, 856
Xu, D. D. et al. 2009, MNRAS, 398, 1235
Zehavi, I. et al. 2011, ApJ, 736, 59
Zentner, A. R., Berlind, A. A., Bullock, J. S., Kravtsov, A. V., & Wechsler, R. H. 2005, ApJ, 624, 505
Zheng, Z. et al. 2005, ApJ, 633, 791